Research Report

Lattice Boltzmann Method for the Convection-diffusion Equation

Hiroaki Yoshida and Makoto Nagaoka

■**ABSTRACT**‖ A numerical scheme based on the lattice Boltzmann method for analyzing the convection-diffusion equation is reviewed in the present paper. The main focus is on the collision operator used in the lattice Boltzmann method. The most widely used operator is the classical Bathnagar-Gross-Krook (BGK) operator, which is simple and easy to use for programming. In engineering applications, however, it suffers from some limitations, such as unexpectedly large computational errors under severe conditions and the incapability of capturing the anisotropic diffusion process. The multiple-relaxation-time (MRT) collision operator has been recently proposed to overcome these drawbacks of the BGK operator. The present paper overviews the lattice Boltzmann scheme using the MRT collision operator, including a detailed numerical procedure. Several numerical examples are also shown, in which specific problems consisting of the convection-diffusion equation and Dirichlet and/or Neumann boundary conditions are analyzed. In addition, an alternative treatment for the Neumann-type boundary condition that improves the accuracy on a curved boundary is presented along with numerical demonstrations.

■**KEYWORDS**‖ Lattice Boltzmann Method, Multiple Relaxation Times,
Convection-diffusion Equation, Anisotropy, Asymptotic Analysis

1. Introduction

The lattice Boltzmann method (LBM)[1,2] has emerged as an alternative numerical method for solving the Navier–Stokes type equations and has been extended to various types of flows, for example, turbulence,[3,4] multi-phase systems,[5,6] flows of multi-component fluids,[7,8] micro scale flows,[9,10] and flows through porous media.[11,12] Attempts have also been made to use the LBM to solve the convection-diffusion equation and related equations, such as the pure diffusion equation and the Poisson equation.[13-17] Although there are a vast number of alternative schemes for these equations associated with the finite element or finite-difference methods, the LBM is nevertheless attractive because it is easy to use for programming and is compatible with parallel computing. In addition, when we consider the diffusion phenomena in complex morphology, such as ion transport in fuel cells[18,19] and secondary batteries,[20] the LBM is a promising tool in view of the success in flows through porous media.

Most of the lattice Boltzmann models for the convection-diffusion equation are commonly limited to isotropic diffusion. This is because the Bathnagar-Gross-Krook (BGK) type model, which is the most commonly used collision model in the LBM, does not have sufficient parameters to describe anisotropic diffusion. Since anisotropy of diffusion plays a critical role in a variety of applications (see, e.g., Refs. (21),(22)), removing this limitation is important. Recently, several groups have developed lattice Boltzmann models for anisotropic diffusion.[23-27] In particular, Ref. (25) two types of models, referred to as equilibrium- and link-type models, with various sets of discrete velocities in two and three dimensions are described. These models can incorporate full anisotropy with off-diagonal components of the diffusion-coefficient tensor. However, the simplest models with five discrete velocities in two dimensions (D2Q5) and seven discrete velocities in three dimensions (D3Q7) are limited to the case of diagonal diffusion-coefficient tensors (DnQm denotes m discrete velocities in n dimensions).

Recently, an LBM for the CDE, which is based on the multiple-relaxation-time (MRT) collision operator, has been proposed.[28] Although the method requires only seven discrete velosities (D3Q7), the number of tunable parameters is sufficient to cover the anisotropic diffusion-coefficient tensor. Therefore, the overhead in memory and CPU time is small compared to that of other existing methods using larger numbers of discrete velocities, such as D3Q15 and D3Q19. The boundary treatment is also simple compared to that for

other models,[29-31] which further facilitates the implementation of the algorithm. In the present paper, we overview the lattice Boltzmann method proposed in Ref. (28) including a detailed numerical procedure.

In engineering applications that involve complex geometries, the boundaries of the computational domain are curved.[18-20] In such cases, however, the straightforward application of the simple rule for the Neumann-type boundary condition mentioned above fails to capture the correct behavior of the macroscopic quantities, i.e., the numerical approximation does not converge to the exact solution no matter how high we make the grid resolution. This inherent difficulty stems from the fact that the surface area is overestimated when the boundary is approximated by the collection of cube surfaces. We present an alternative treatment for curved Neumann-type boundaries, which circumvents this difficulty by introducing the local specific surface area. The signed distance function handled by the level set method (see, e.g., Ref. (32)) is used in the present paper to estimate the local specific surface area. We demonstrate the improvement by performing a numerical experiment for a simple problem with a reactive sphere. The numerical result of the electrical potential field in a reactive porous medium is also shown as an example of a practical application.

2. Lattice Boltzmann Method

2. 1 Convection-diffusion Equation

First of all, we specify the partial differential equation to be solved by using the lattice Boltzmann method, which is the convection-diffusion equation (CDE) for the scalor variable $\varphi(t, \mathbf{x})$ on a domain $\Omega \subset R^3$ with an initial condition:

$$\frac{\partial \varphi}{\partial t} + \frac{\partial}{\partial x_j}(\varphi v_j) = \frac{\partial}{\partial x_i}\left(D_{ij}\frac{\partial \varphi}{\partial x_j}\right) + S, \cdots \cdots (1)$$

$$\varphi(0, \mathbf{x}) = \psi(\mathbf{x}), \cdots \cdots \cdots \cdots \cdots \cdots \cdots (2)$$

where $t \in [0, T]$ is the time, and $\mathbf{x} \in R^3$ is the spatial coordinate. (We either use boldface letters or assign indexes i, j, and k to designate the vector element in R^3. We assume the summation convention for repeated indexes.) The (anisotropic) diffusion coefficient D_{ij} is a positive definite symmetric matrix. The background velocity $\mathbf{v}(t, \mathbf{x})$, which is a given function, is assumed

to be divergence-free. The given functions $S(\varphi)$ and $\psi(\mathbf{x})$ are the source term and the initial condition, respectively.

We consider two types of boundary conditions in the present paper: on the boundary $\partial\Omega_d \subset \partial\Omega$, the Dirichlet boundary value is specified:

$$\varphi = \Phi_d, \cdots \cdots \cdots \cdots \cdots \cdots \cdots \cdots \cdots (3)$$

and on the boundary $\partial\Omega_n \subset \partial\Omega$, the Neumann-type boundary condition (the flux-specified condition) is imposed:

$$-n_i D_{ij}\frac{\partial \varphi}{\partial x_j} + n_j v_j \varphi = \Phi_n, \cdots \cdots \cdots \cdots (4)$$

where $\mathbf{n}$ is the unit normal vector on pointing inward to the domain.

2. 2 Lattice Boltzmann Equation

In the lattice Boltzmann method, the behavior of the distribution function $f_\alpha(t, \mathbf{x})$, where $\alpha = 0, 1, 2,..., 6$, is tracked on the basis of the lattice Boltzmann equation (LBE). The sum of the distribution function $\varphi = \Sigma_\alpha f_\alpha$ approximates the solution of the CDE. The distribution function f_α is transported over a regular spatial lattice with assigned discrete velocities $\mathbf{e}_\alpha$ (see **Fig. 1**):

$$[\mathbf{e}_0, \mathbf{e}_1, \mathbf{e}_2, \mathbf{e}_3, \mathbf{e}_4, \mathbf{e}_5, \mathbf{e}_6] = \begin{bmatrix} 0 & 1 & -1 & 0 & 0 & 0 & 0 \\ 0 & 0 & 0 & 1 & -1 & 0 & 0 \\ 0 & 0 & 0 & 0 & 0 & 1 & -1 \end{bmatrix}.$$

$$\cdots \cdots \cdots \cdots \cdots (5)$$
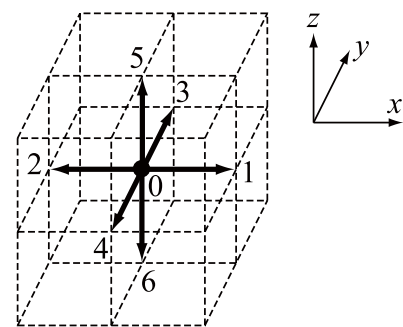
Fig. 1   Seven-velocity model in three dimensions (D3Q7 model).

We use Greek subscripts to indicate the quantities corresponding to the directions of the discrete velocities, as f_α above.

The LBE is written in the following form:

$$f_\alpha(t + \Delta t, \mathbf{x} + \mathbf{e}_\alpha \Delta x) - f_\alpha(t, \mathbf{x}) = L(f)_\alpha + \Delta t S \omega_\alpha,$$
$$\cdots\cdots\cdots\cdots\cdots\cdots (6)$$

where Δt and Δx are the time step and the grid interval, respectively. Here, ω_α is the weight coefficient defined in Eq. (10) below. The operator L is referred to as the collision operator, defines how the f_α's interact during a time step. In the next subsection, an explicit expression of the collision operator of the BGK model is presented, and we later define the MRT collision operator.

2. 3 BGK Collision Operator

The most widely used collision operator is the BGK collision operator, which has the following form:

$$L(f)_\alpha = \frac{1}{\tau}(f_\alpha^{eq} - f_\alpha), \cdots\cdots\cdots\cdots\cdots (7)$$

where τ is a coefficient that represents the relaxation time relative to the time step. In this operator, all the components of f_α relax to the equilibrium f_α^{eq} with the single relaxation time. In solving the CDE, f_α^{eq} is defined as follows:

$$f_\alpha^{eq} = (\omega_\alpha + \frac{\Delta t}{\Delta x \Lambda} v_j e_{\alpha j} \omega_\alpha)\varphi, \cdots\cdots\cdots\cdots (8)$$

$$\varphi = \sum_\alpha f_\alpha \cdots\cdots\cdots\cdots\cdots\cdots\cdots\cdots (9)$$

Here, the weight coefficient ω_α is defined as

$$\omega_\alpha = \begin{cases} 1/4, & (\alpha = 0) \\ 1/8, & (\alpha = 1,...,6) \end{cases} \cdots\cdots\cdots\cdots (10)$$

and the coefficient included in Eq. (8) is $\Lambda = 1/4$.

2. 4 Multiple-relaxation-time Collision Operator

The basic idea for the multiple-relaxation-time (MRT) collision operator is that the relaxation process is operated on the transformed vector space which is referred to as the moment space. (For MRT operators for flow simulations, see, e.g., Refs.(33)-(35).) More specifically, the vector f_α in the original seven-dimensional vector space is projected onto the space in which each component corresponds to a certain moment of f_α. Then, each component relaxes to the equilibrium with a different relaxation coefficient. The result of relaxation is projected back onto the original seven-dimensional space. In contrast to the BGK model with the single relaxation coefficient, the MRT model allows us to tune the relaxation coefficient for each moment separately, and thus we are able to take anisotropy into account.

The collision operator in Eq. (6) for the MRT collision operator is defined as follows[28]:

$$L(f)_\alpha = \sum_\beta (M^{-1}QM)_{\alpha\beta}(f_\beta^{eq} - f_\beta), \cdots\cdots\cdots (11)$$

where the definition of f_α^{eq} is given by Eq. (8). Here, M is the matrix that projects a vector onto the moment space, defined as

$$M = \begin{pmatrix} 1 & 1 & 1 & 1 & 1 & 1 & 1 \\ 0 & 1 & -1 & 0 & 0 & 0 & 0 \\ 0 & 0 & 0 & 1 & -1 & 0 & 0 \\ 0 & 0 & 0 & 0 & 0 & 1 & -1 \\ 6 & -1 & -1 & -1 & -1 & -1 & -1 \\ 0 & 2 & 2 & -1 & -1 & -1 & -1 \\ 0 & 0 & 0 & 1 & 1 & -1 & -1 \end{pmatrix}.$$
$$\cdots\cdots\cdots\cdots\cdots (12)$$

The relaxation-time matrix Q is then defined in the following form:

$$Q^{-1} = \begin{pmatrix} \tau_0 & 0 & 0 & 0 & 0 & 0 & 0 \\ 0 & \bar{\tau}_{xx} & \bar{\tau}_{xy} & \bar{\tau}_{xz} & 0 & 0 & 0 \\ 0 & \bar{\tau}_{xy} & \bar{\tau}_{yy} & \bar{\tau}_{yz} & 0 & 0 & 0 \\ 0 & \bar{\tau}_{xz} & \bar{\tau}_{yz} & \bar{\tau}_{zz} & 0 & 0 & 0 \\ 0 & 0 & 0 & 0 & \tau_4 & 0 & 0 \\ 0 & 0 & 0 & 0 & 0 & \tau_5 & 0 \\ 0 & 0 & 0 & 0 & 0 & 0 & \tau_6 \end{pmatrix}.$$
$$\cdots\cdots\cdots\cdots\cdots (13)$$

It should be noted that the relaxation-time matrix has the off-diagonal components, which correspond to the

rotation of the principal axis of anisotropic diffusion. If we set the values of the coefficients $\overline{\tau}_{ij}$ as in Eq. (14) below, the φ obtained using the proposed model approaches the solution to the CDE as $\Delta x \to 0$, while maintaining $\Delta t / \Delta x^2 = const.$:

$$\overline{\tau}_{ij} = \frac{1}{2}\delta_{ij} + \frac{\Delta t}{\Lambda \Delta x^2} D_{ij}, \quad \cdots\cdots\cdots\cdots\cdots (14)$$

where δ_{ij} is the Kronecker delta. The relaxation coefficient τ_0 for the conserved quantity φ does not affect the numerical solution, while the components τ_4, τ_5, and τ_6, have no effect on the leading-order approximation of the CDE solution, but they do affect the error terms.

2. 5　Computational Procedure

In this subsection, the procedure for the implementation of the LBM is presented. Initialization and the boundary rules are also described.
(i). Initial distribution: the initial distribution is expressed in terms of the initial condition $\psi(\mathbf{x}) = \varphi(0, \mathbf{x})$ as follows:

$$f_\alpha(0, \mathbf{x}) = \omega_\alpha \psi + \omega_\alpha e_{\alpha j} \frac{\Delta t v_j}{\Delta x \Lambda} \psi. \quad \cdots\cdots\cdots\cdots (15)$$

If the initial condition $\psi(\mathbf{x})$ includes a gradient, a slight correction to the above equation is necessary to maintain accuracy.[28]
(ii). Collision: the distribution function after the collision process, denoted by $\hat{f}_\alpha$, is given by

$$\hat{f}_\alpha(t, \mathbf{x}) = f_\alpha(t, \mathbf{x}) + L(f)_\alpha(t, \mathbf{x}) + \Delta t S \omega_\alpha.$$
$$\cdots\cdots\cdots\cdots\cdots (16)$$

(iii). Streaming: the value of $\hat{f}_\alpha$ is moved in the direction of $\mathbf{e}_\alpha$ by the distance Δx:

$$f_\alpha(t + \Delta t, \mathbf{x} + \mathbf{e}_\alpha \Delta x) = \hat{f}_\alpha(t, \mathbf{x}). \quad \cdots\cdots\cdots (17)$$

(iv). Dirichlet boundary condition: if the node from which the distribution function streams $(\mathbf{x} - \mathbf{e}_\alpha \Delta x)$ is outside the domain Ω through $\partial\Omega_d$, then the value of $f_\alpha(t + \Delta t, \mathbf{x})$ is given by the rule

$$f_\alpha(t + \Delta t, \mathbf{x}) = -\hat{f}_\beta(t, \mathbf{x}) + \Lambda \Phi_d. \quad \cdots\cdots\cdots (18)$$

Here, and in what follows, the index β indicates the direction opposite to α, i.e., $\mathbf{e}_\alpha = -\mathbf{e}_\beta$.
(v). Neumann-type boundary condition: if the node from which the distribution function streams $(\mathbf{x} - \mathbf{e}_\alpha \Delta x)$ is outside the domain Ω through $\partial\Omega_n$, then the following rule applies:

$$f_\alpha(t + \Delta t, \mathbf{x}) = \hat{f}_\beta(t, \mathbf{x}) + \Delta t \Phi_n / \Delta x. \quad \cdots\cdots\cdots (19)$$

(vi). Macroscopic quantity: the value of φ is computed from Eq. (9) using the updated f_α.
(vii). Processes (ii)–(vi) are repeated until $t + \Delta t$ reaches T, or a specified convergence condition is satisfied in steady problems.

3. Asymptotic Analysis

In this section, we briefly describe how the numerical solution obtained from the LBM is proven to approximate the solution of the target partial differential equation, i.e., the CDE. (A more detailed description is presented in Ref. (28).) The classical Chapman-Enskog expansion technique is the most widely used protocol to investigate the convergence of the LBM (see, e.g., Refs. (1),(16),(25),(36)). Recently, a similar but essentially different technique referred to as asymptotic analysis has been proposed by Junk et al.[37,38] Although the former is a powerful tool to show that the LBE reproduces certain partial differential equations, the dependence of the numerical solution on the expansion parameter is not immediately clear.[39] On the other hand, in asymptotic analysis, the numerical solution itself is expanded in terms of powers of the small parameter representing the grid interval, and is analyzed order by order in the expansion. Therefore, clear information about the structure of the numerical solution is revealed. We have performed asymptotic analysis on the lattice Boltzman algorithm described in the previous section, and we have found that the leading order term in the expansion $\varphi = \varphi^{(0)} + \varphi^{(1)}\varepsilon + \varphi^{(2)}\varepsilon^2 \cdots$, where $\varepsilon = \Delta x / $ (characteristic length), satisfies the CDE (1). Furthermore, the analysis of the higher-order terms has shown that the present model is first- and second-order accurate in time and space, respectively.[28]

4. Numerical Examples

In this section, the LBM described in Section 2 is applied to a few specific problems. In Section 4.1, we

verify the applicability of the method to problems with various types of boundary conditions. We also investigate the dependence of the error on the relaxation coefficient. In the second example, the anisotropic diffusion-coefficient tensors are considered. In Section 4.3, we consider curved boundaries on which the flux of φ is specified. A boundary rule to improve accuracy for curved boundaries, which replaces Eq. (19), is also presented.

4.1 Helmholtz Equation

First, we consider the Helmholtz equation in the bounded domain:

$$\frac{\partial^2 \varphi}{\partial x_j^2} = \kappa^2 \varphi, \quad x, y, z \in [0,1]. \quad \cdots \cdots \cdots \cdots (20)$$

The boundary conditions are

$$\frac{\partial \varphi}{\partial x}(0, y, z) = -\mu \cos \pi y \sin \pi z, \quad \varphi(1, y, z) = 0,$$
$$\cdots \cdots \cdots \cdots \cdots (21)$$

$$\varphi(x, 0, z) = \frac{\sinh \mu (1-x) \sin \pi z}{\cosh \mu},$$

$$\varphi(x, 1, z) = -\frac{\sinh \mu (1-x) \sin \pi z}{\cosh \mu},$$
$$\cdots \cdots \cdots \cdots \cdots (22)$$

$$\varphi(x, y, 0) = 0, \quad \varphi(x, y, 1) = 0, \quad \cdots \cdots \cdots \cdots \cdots (23)$$

where $\mu = \sqrt{\kappa^2 + 2\pi^2}$. This boundary-value problem has the following exact solution:

$$\varphi_{exact} = \frac{\sinh \mu (1-x) \cos \pi y \sin \pi z}{\cosh \mu}. \quad \cdots \cdots \cdots (24)$$

We implement the LBM simulation with the initial condition $\varphi = 0$ and regard the steady state as the numerical solution to the above problem. Since, in this case, the diffusion-coefficient tensor is $D_{ij} = \delta_{ij}$, the form of the corresponding relaxation coefficients is $\bar{\tau}_{ij} = \tau_D \delta_{ij}$ (see Eq. (14)). The relaxation coefficients that have no physical significance, i.e., τ_0, τ_4, τ_5, and τ_6, can be set independently of $\bar{\tau}_{ij} = \tau_D \delta_{ij}$. Throughout this section, the value of these coefficients is fixed at unity ($\tau_p = 1$ ($p = 0,4,5,6$)). The accuracy of the numerical solution is measured by using the error between the numerical solution $\varphi_{numerical}$ and the exact solution:

$$E_2 = \left((1/N^3) \sum_{x,y,z} (\varphi_{numerical} - \varphi_{exact})^2 \right)^{1/2}.$$

We show in **Fig. 2**(a) the log-log plot of E_2 versus the grid interval $\varepsilon = 1/N$ for the case in which $\kappa = \pi$. The results show second-order accuracy with respect to the grid interval, as mentioned in the previous section. (The slope equal to 2 is indicated in the figure.) The error increases as the value of τ_D increases. In order to examine the dependence of the error on τ_D in greater detail, we show E_2 versus τ_D for $\varepsilon = 0.025$ in
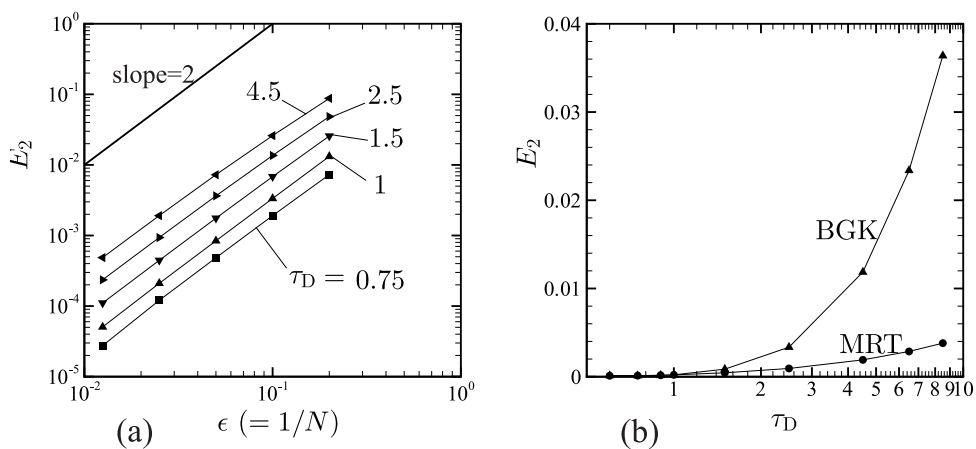
Fig. 2   (a) E_2 versus $\varepsilon = 1/N$ for various values of τ_D for the case of the Helmholtz equation. The results of the multiple-relaxation-time (MRT) model are shown. The line indicating a slope of 2 is also shown in the figure. (b) E_2 versus τ_D for $\varepsilon = 0.025$ for the case of the Helmholtz equation. The results of the multiple-relaxation-time (MRT) model and the Bathnagar-Gross-Krook (BGK) model are shown.

Fig. 2(b). For comparison, the results obtained using the BGK model are also shown in Fig. 2(b). Clearly, the MRT collsion model suppresses the rate of error increase.

As demonstrated by this example, the MRT collision model makes the numerical error less sensitive to the relaxation coefficient $\bar{\tau}_{ij} = \tau_D \delta_{ij}$. This is because keeping $\tau_p(p = 4,5,6)$ constant moderates the variation of the higher-order error ($\varphi^{(2)}$). Therefore, even for an isotropic diffusion-coefficient, the MRT model is still beneficial if τ_D is large. In the example of this subsection, increasing the value of τ_D corresponds to increasing the value of Δt because the relation (14) holds. Thus, Fig. 2(b) suggests that the computational time can be reduced using the MRT model with a larger value of Δt. For instance, if we allow the error to be comparable to that of the BGK model for $\tau_D =$ 2.5 in **Fig. 3**, we can enlarge τ_D up to 8.5, which means that Δt can be four times as large as that for the BGK model (see Eq. (14)). The MRT model will also exhibit

this advantage for the case in which the diffusion-coefficient varies temporally and/or spatially because τ_D can be large in such cases owing to the relation (14).

4. 2 Convection and Anisotropic Diffusion of a Gaussian Hill

Next, we consider the time evolution of a Gaussian hill under a uniform flow. The x coordinate is taken along the flow, and the origin of the coordinates is at the center of the initial Gaussian, i.e., $\mathbf{v} = (v_x,0,0)$ and

$$\varphi(0, \mathbf{x}) = \frac{\varphi_0}{(2\pi\sigma_0^2)^{3/2}} \exp\left(-\frac{x_j^2}{2\sigma_0^2}\right), \cdots \cdots \cdots (25)$$

where φ_0 is the total concentration, and σ_0^2 is the initial variance. The initial-value problem, Eq. (1) without the source term and Eq. (25), has the following exact solution:

(a) initial condition

(b) isotropic

(c) diagonally anisotropic

(d) fully anisotropic
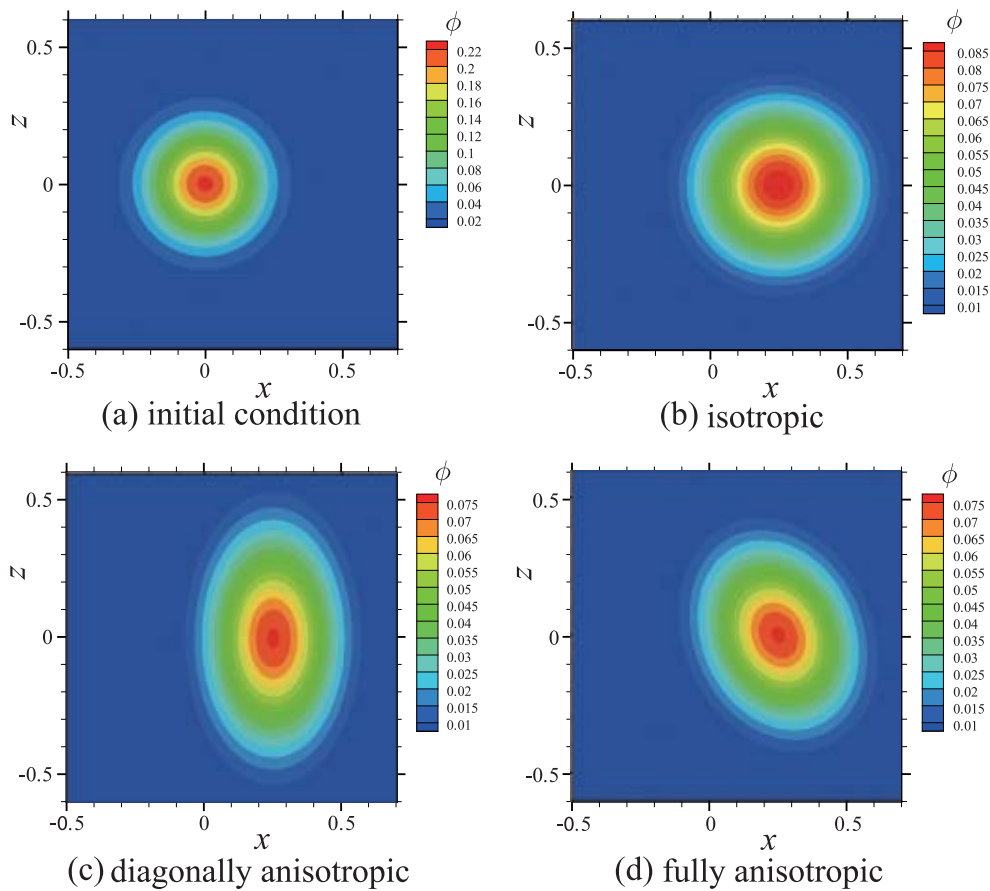
Fig. 3   Convection and diffusion of a Gaussian hill. $\varphi_0 = 0.01$, $\sigma_0^2 = 0.02$, $v_x = 10$, and $N = 64$. The initial profile of φ in the x-z plane at $y = 0$ is shown in (a), and the corresponding profiles at $t = 0.025$ are shown in (b), (c), and (d). The diffusion-coefficient tensor is isotropic in (b), diagonally anisotropic in (c), and fully anisotropic in (d) (see Eq. (27)).

$$\varphi_{exact}(t, \mathbf{x}) = \frac{\varphi_0}{(2\pi)^{3/2} \| \sigma_{ij} \|^{1/2}} \exp\left(-\frac{(\sigma^{-1})_{ij}(x_i - v_i t)(x_j - v_j t)}{2} \right),$$

$$\cdots\cdots\cdots\cdots\cdots (26)$$

where $\sigma_{ij} = \sigma_0^2 \delta_{ij} - 2t D_{ij}$; $\| \sigma_{ij} \|$ is the absolute value of the determinant of σ_{ij}, and $(\sigma^{-1})_{ij}$ is the (i, j) component of the inverse of σ_{ij}.

In order to test the applicability to anisotropic diffusion, we consider the following three types of diffusion-coefficient tensors:

$$D_{ij} = \begin{pmatrix} 25^{-1/3} & 0 & 0 \\ 0 & 25^{-1/3} & 0 \\ 0 & 0 & 25^{-1/3} \end{pmatrix}, \begin{pmatrix} \dfrac{1}{10} & 0 & 0 \\ 0 & \dfrac{2}{5} & 0 \\ 0 & 0 & 1 \end{pmatrix},$$

$$\begin{pmatrix} \dfrac{1}{4} & -\dfrac{3\sqrt{2}}{40} & -\dfrac{3\sqrt{2}}{40} \\ -\dfrac{3\sqrt{2}}{40} & \dfrac{5}{8} & -\dfrac{3}{8} \\ -\dfrac{3\sqrt{2}}{40} & -\dfrac{3}{8} & \dfrac{5}{8} \end{pmatrix}. \cdots\cdots\cdots (27)$$

The second type of diffusion-coefficient tensor possesses diagonal anisotropy, whereas the third type of diffusion-coefficient tensor has full anisotropy with off-diagonal components. The third tensor is the rotation of the second tensor by angle of $\pi / 6$ about z and x axes, in this order. The relaxation coefficients are related to these diffusion-coefficient tensors via Eq. (14).

The numerical results for the case of $\varphi_0 = 0.01$, $\sigma_0^2 = 0.02$, and $v_x = 10$ are shown in Fig. 3. In the figure, the profiles of φ at $t = 0.025$ in the x-z plane at $y = 0$ are shown, and the initial profile in the same plane is also shown in Fig. 3(a). Figures 3(c) and (d) show that the present LBM successfully captures the convection and anisotropic diffusion process. Since the profile of φ is quite local in this problem, E_∞ defined below is more appropriate for investigating the accuracy: $E_\infty = \max_{x,y,z} |\varphi_{numerical} - \varphi_{exact}|$. We plot E_∞ as a function of $\varepsilon = 1 / N$ in **Fig. 4**. The values of the parameters used here are the same as those in Fig. 3. The figure confirms that the second-order accuracy of the present model is not violated by the anisotropy of the diffusion-coefficient tensor.

4. 3 Surface Reaction on a Sphere

The final example involves a surface reaction on a sphere. Here, we consider the cubic domain $\Omega = \{\mathbf{x} \,|\, x \in [0, 2]; y, z \in [-1, 1]\}$. On the boundaries at $x = 0$ and $x = 2$, the concentration is fixed at $\varphi = 1$ and $\varphi = 0$, respectively, and the Neumann-type condition with no flux is assumed on the rest of the boundaries. A sphere with radius R is located at the center of the domain. The surface reaction takes place on the sphere boundary $\partial\Omega_s = \{\mathbf{x} \,|\, (x-1)^2 + y^2 + z^2 = R^2\}$. The concentration flux is given by

$$-n_j D \frac{\partial \varphi}{\partial x_j} = J_n, \quad \mathbf{x} \in \partial\Omega_s, \cdots\cdots\cdots\cdots (28)$$

where n is the unit normal vector pointing inward to the domain, and D is the diffusion coefficient, which is assumed to be isotropic in this example. Neither convection nor bulk reaction are considered here, i.e., $\mathbf{v} = 0$ and $S = 0$.

Let us denote by $\Delta \bar{J}$ the difference between the total fluxes flowing through the two fixed-concentration boundaries. The conservation law implies that in the steady state $\Delta \bar{J}$ is equal to the total flux from the sphere: $\Delta \bar{J} = 4\pi R^2 J_n$. We use this relation for validation of the model. If we straightforwardly apply the procedure described in Section 2.5 to the present problem, the conservation law described above is not
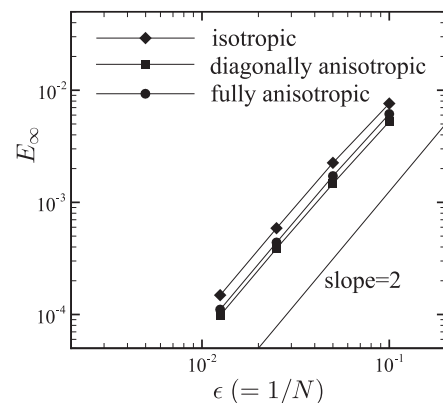
Fig. 4 E_∞ evaluated at $t = 0.025$ versus $\varepsilon = 1 / N$ for the case of convection and diffusion of a Gaussian hill. The results for the cases of isotropic ($\blacklozenge$), diagonally anisotropic ($\blacksquare$), and fully anisotropic ($\bullet$) diffusion-coefficient tensors are shown. The line indicating a slope of 2 is also shown in the figure. See the caption of Fig. 3 for the other parameters.

satisfied accurately, as shown in **Fig. 5**. The symbol ■ indicates the results obtained using the rule in Eq. (19). The solid line indicates the analytical expression, i.e., $\Delta \overline{J} = 4\pi R^2 J_n$. The disagreement arises from the fact that the surface area on which the reaction occurs is overestimated. More specifically, the surface of the sphere is approximated by the set of the cube surfaces with side length Δx when Eq. (19) is used. No matter how small we make Δx, the approximated area does not converge to the exact value. To avoid this difficulty, we use an alternative treatment for curved boundaries, as described below.

In the modified treatment, procedure (v) in Section 2.5 is replaced by

- If $\mathbf{x} - \mathbf{e}_\alpha \Delta x$ is outside the cell boundary that envelopes the domain Ω (the thick line in **Fig. 6**(a)), then the rule in Eq. (19) with $\Phi_n = 0$ (the bounce-back rule) is applied. (The *cell* of a lattice point refers to the cube box with side length Δx, the center of which is located at the lattice point.) Subsequently, on the lattice points of cells that intersects the boundary (○ in Fig. 6(a)), Δf_α defined below is further added to f_α:

$$\Delta f_\alpha = \begin{cases} \dfrac{A \Phi_n \Delta t}{\Delta x} \dfrac{(\mathbf{e}_\alpha \cdot \mathbf{n})}{\sum_\gamma \mathbf{e}_\gamma \cdot \mathbf{n}}, & \text{if } \mathbf{e}_\alpha \cdot \mathbf{n} > 0 \\ 0, & \text{otherwise} \end{cases} , \quad \cdots \ (29)$$

where $A = A_c / \Delta x^2$, with A_c being the area of the intersection between the cell and the boundary. The summation is taken over γ such that $\mathbf{e}_\gamma \cdot \mathbf{n} > 0$.

In the actual implementation of the above procedure, we clearly need to prepare the normal $\mathbf{n}$ and the local specific surface area A assigned to each lattice point

around the boundary. The signed distance function $\phi(\mathbf{x})$ handled by the level set method [32] can be used for preparation of $\mathbf{n}$ and A. The value of ϕ indicates the distance from the boundary ($\phi = 0$ for $\mathbf{x} \in \partial\Omega$), and the sign corresponds to the phase. We can obtain the value of ϕ, immediately if the boundary is expressed in an analytical form. On the other hand, if a set of binary voxel data approximating the shape of Ω is given, ϕ is obtained by applying an appropriate re-distancing procedure using the voxel data as the initial condition (see, e.g., Refs. (32),(40)). The normal $\mathbf{n}$ is obtained by taking the gradient of ϕ, and the area A_c is approximated by the area of the intersection between the cell and the plane normal to $\mathbf{n}$ displaced by the
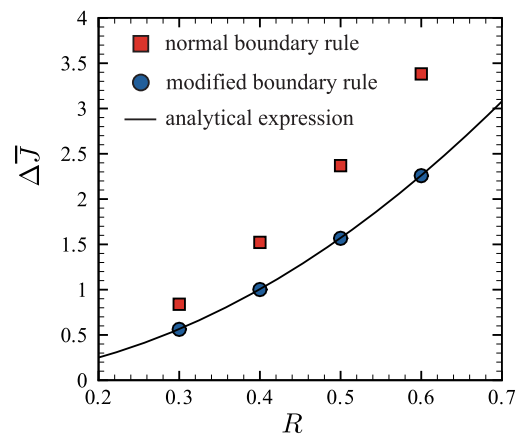
Fig. 5　Reaction flux from the sphere. $\Delta \overline{J}$ versus R for $D = 1$ and $J_n = 0.5$. The symbol ■ indicates the results obtained using the normal boundary rule (19), and ● indicates the results obtained using the modified boundary rule described in Section 4.3. The solid line indicates the analytical expression.

(a)　　　　　　　　　　　(b)

Fig. 6　(a) A two-dimensional schematic diagram of the lattice points around the curved boundary. The solid grid lines indicate the cell boundary, and the thick line indicates the cell boundary enveloping Ω. The black circle ● depicts the normal lattice points, and the white circle ○ depicts the lattice points of the cell that intersects the boundary $\partial\Omega$. (b) Approximated intersection in a cell.
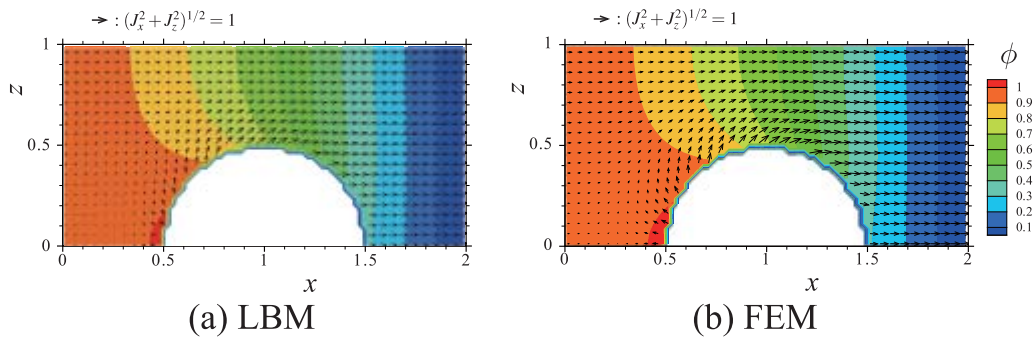
Fig. 7   Profiles of φ and vector fields of (J_x, J_z) in the x-z plane at $y = 0.0125$. $D = 1$, $J_n = 0.5$, and $R = 0.5$. (a) Present lattice Boltzmann method (LBM). (b) Finite element method (FEM).

distance $|\phi|$ from the lattice point (see Fig. 6(b)). For other methods of estimating **n** and A, see, e.g., Ref. (41).

In Fig. 5, the $\Delta \bar{J}$ obtained using the modified rule is also plotted with ●, and exhibits excellent agreement with the exact values. The profile of φ and the vector field of (J_x, J_z) in the x-z plane at $y = 0.0125$ in the case of $R = 0.5$ are shown in **Fig. 7**. For comparison, the corresponding figure obtained using the finite element method (FEM) is also shown. Although satisfactory agreement is achieved, there is a very slight discrepancy of the vectors near the sphere surface. This is because the flux tangential to the boundary surface is exposed to an unphysical restriction due to the bounce-back rule, unless the boundary is parallel to a symmetric axis of the lattice (cf. Ref. (30)). Further modification of the boundary rule to release this restriction, like the attempt made in Ref. (30), may improve the accuracy. Nevertheless, the overall agreement observed in Fig. 7 shows that the rule presented here is sufficient for practical applications.

We have applied the present method to various types of engineering problems such as lithium-ion batteries.[42,43] One example is shown in **Fig. 8**, which is a result of the analysis of the potential field in a reactive porous medium. The governing equation is the same as the case of the single-sphere problem. Although the previous example with a single sphere is simple enough to use the body-fitted mesh in the FEM analysis, it is difficult to establish appropriate mesh systems for the random configuration as shown in Fig. 8. There is still more tough work if the number of simulation cases is large. On the other hand, the LBM supported by the boundary treatment described in this section is straightforwardly applied regardless of the complexity of the boundary.
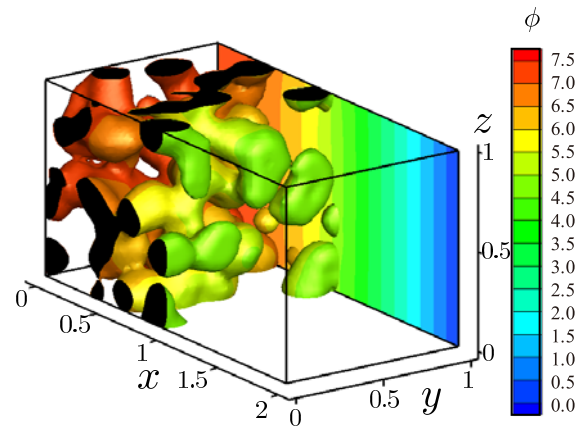
Fig. 8   Potential field in a porous medium. Boundary conditions are as follows: Eq. (28) at the porous surfaces, no-flux condition at $x = 0$, $\varphi = 0$ at $x = 2$, and periodic condition in the y and z directions.

5. Summary

In the present paper, a lattice Boltzmann method for the CDE has been described. The method is a straightforward extension of the classical BGK collision operator to the MRT collision operator. Anisotropy of diffusion, which is not covered by the BGK, is correctly incorporated through the relaxation-time matrix in the MRT collision operator. It was shown analytically and numerically that the lattice Boltzmann algorithm presented in Section 2.5 was second-order accurate with respect to the grid interval.

The ordinary boundary rule for the Neumann-type (specified flux) condition is not sufficiently accurate when the boundary is curved. In order to widen the applicability of the LBM, an improved boundary rule for curved boundaries was developed (Section 4.3). This boundary rule is particularly useful for practical applications that involve complex geometries, such as a random porous structure, because the existing

schemes other than the LBM are not easily applied to such problems. Combined with the improved boundary rule, the LBM reviewed in the present paper is a promising tool for analyzing transport process in complex mesoscopic systems, such as catalysts, fuel cells, and secondary batteries.

References

(1) Chen, S. and Doolen, G. D., "Lattice Boltzmann Method for Fluid Flows", *Annu. Rev. Fluid Mech.*, Vol. 30 (1998), pp. 329-364.

(2) Succi, S., *The Lattice Boltzmann Equation for Fluid Dynamics and Beyond* (2001), Oxford Univ. Press

(3) Lätt, J., Chopard, B., Succi, S. and Toschi, F., "Numerical Analysis of the Averaged Flow Field in a Turbulent Lattice Boltzmann Simulation", *Physica A*, Vol. 362 (2006), pp. 6-10.

(4) Yu, H., Luo, L.-S. and Girimaji, S. S., "LES of Turbulent Square Jet Flow Using an MRT Lattice Boltzmann Model", *Comput. Fluids*, Vol. 35 (2006), pp. 957-965.

(5) Inamuro, T., Ogata, T., Tajima, S. and Konishi, N., "A Lattice Boltzmann Method for Incompressible Two-phase Flow with Large Density Differences", *J. Comput. Phys.*, Vol. 198 (2004), pp. 628-644.

(6) Zheng, H. W., Shu, C. and Chew, Y. T., "A Lattice Boltzmann Model for Multiphase Flows with Large Density Ratio", *J. Comput. Phys.*, Vol. 218 (2006), pp. 353-371.

(7) Luo, L. -S. and Girimaji, S. S., "Theory of the Lattice Boltzmann Method: Two-fluid Model for Binary Mixtures", *Phys. Rev. E*, Vol. 67 (2003), 036302.

(8) Asinari, P., "Asymptotic Analysis of Multiple-relaxation-time Lattice Boltzmann Schemes for Mixture Modeling", *Comput. Math. Appl.*, Vol. 55 (2008), pp. 1392-1407.

(9) Guo, Z., Zhao, T. S. and Shi, Y., "Physical Symmetry, Spatial Accuracy, and Relaxation Time of the Lattice Boltzmann Equation for Microgas Flows", *J. Appl. Phys.*, Vol. 99 (2006), 074903.

(10) Niu, X. -D., Hyodo, S., Munekata, T. and Suga, K., "Kinetic Lattice Boltzmann Method for Microscale Gas Flows: Issues on Boundary Condition, Relaxation Time, and Regularization", *Phys. Rev. E*, Vol. 76 (2007), 036711.

(11) Guo, Z. and Zhao, T. S., "Lattice Boltzmann Model for Incompressible Flows through Porous Media", *Phys. Rev. E*, Vol. 66 (2002), 036304.

(12) Kang, Q., Lichtner, P. C. and Zhang, D., "An Improved Lattice Boltzmann Model for Multicomponent Reactive Transport in Porous Media at the Pore Scale", *Water Resour. Res.*, Vol. 43 (2007), W12S14.

(13) Flekkøy, E. G., "Lattice Bhatnagar-Gross-Krook Models for Miscible Fluids", *Phys. Rev. E*, Vol. 47 (1993), pp. 4247-4257.

(14) Wolf-Gladrow, D., "A Lattice Boltzmann Equation for Diffusion", *J. Stat. Phys.*, Vol. 79 (1995), pp. 1023-1032.

(15) Stockman, H. W., Glass, R. J., Cooper, C. and Rajaram, H., "Accuracy and Computational Efficiency in 3D Dispersion via Lattice-Boltzmann: Models for Dispersion in Rough Fractures and Double-diffusive Fingering", *Int. J. Mod. Phys. C*, Vol. 9 (1998), pp. 1545-1557.

(16) Shi, B. C., Deng, B., Du, R. and Chen, X. W., "A New Scheme for Source Term in LBGK Model for Convection-diffusion Equation", *Comput. Math. Appl.*, Vol. 55 (2008), pp. 1568-1575.

(17) Shi, B. C. and Guo, Z., "Lattice Boltzmann Model for Nonlinear Convection-diffusion Equations", *Phys. Rev. E*, Vol. 79 (2009), 016701.

(18) Asinari, P., Quaglia, M. C., von Spakovsky, M. R. and Kasula, B. V., "Direct Numerical Calculation of the Kinematic Tortuosity of Reactive Mixture Flow in the Anode Layer of Solid Oxide Fuel Cells by the Lattice Boltzmann Method", *J. Power Sources*, Vol. 170 (2007), pp. 359-375.

(19) Suzue, Y., Shikazono, N. and Kasagi, N., "Micro Modeling of Solid Oxide Fuel Cell Anode Based on Stochastic Reconstruction", *J. Power Sources*, Vol. 184 (2008), pp. 52-59.

(20) Wang, C. -W. and Sastry, A. M., "Mesoscale Modeling of a Li-Ion Polymer Cell", *J. Electrochem. Soc.*, Vol. 154 (2007), pp. A1035-A1047.

(21) Link, S., Chang, W. -S., Yethiraj, A. and Barbara, P. F., "Anisotropic Diffusion of Elongated and Aligned Polymer Chains in a Nematic Solvent", *J. Phys. Chem. B*, Vol. 110 (2006), pp. 19799-19803.

(22) Johnson, P. M., Faez, S. and Lagendijk, A., "Full Characterization of Anisotropic Diffuse Light", *Opt. Express*, Vol. 16 (2008), pp. 7435-7446.

(23) Zhang, X., Bengough, A. G., Crawford, J. W. and Young, I. M., "A Lattice BGK Model for Advection and Anisotropic Dispersion Equation", *Adv. Water Resour.*, Vol. 25 (2002), pp. 1-8.

(24) Zhang, X., Bengough, A. G., Deeks, L. K., Crawford, J. W. and Young, I. M. "A Novel Three-dimensional Lattice Boltzmann Model for Solute Transport in Variably Saturated Porous Media", *Water Resour. Res.*, Vol. 38 (2002), pp. 1167-1177.

(25) Ginzburg, I., "Equilibrium-type and Link-type Lattice Boltzmann Models for Generic Advection and Anisotropic-dispersion Equation", *Adv. Water Resour.*, Vol. 28 (2005), pp. 1171-1195.

(26) Rasin, I., Succi, S. and Miller, W., "A Multi-relaxation Lattice Kinetic Method for Passive Scalar Diffusion", *J. Comput. Phys.*, Vol. 206 (2005), pp. 453-462.

(27) Suga, S., "Stability and Accuracy of Lattice Boltzmann Schemes for Anisotropic Advection-diffusion Equations", *Int. J. Mod. Phys. C*, Vol. 20 (2009), pp. 633-650.

(28) Yoshida, H. and Nagaoka, M., "Multiple-relaxation-time Lattice Boltzmann Model for the Convection

and Anisotropic Diffusion Equation", *J. Comput. Phys.*, Vol. 229 (2010), pp. 7774-7795.

(29) He, X., Li, N. and Goldstein, B., "Lattice Boltzmann Simulation of Diffusion-convection Systems with Surface Chemical Reaction", *Mol. Simulat.*, Vol. 25 (2000), pp. 145-156.

(30) Ginzburg, I., "Generic Boundary Conditions for Lattice Boltzmann Models and their Application to Advection and Anisotropic Dispersion Equations", *Adv. Water Resour.*, Vol. 28 (2005), pp. 1196-1216.

(31) Akinaga, Y., Hyodo, S. and Ikeshoji, T., "Lattice Boltzmann Simulations for Proton Transport in 2-D Model Channels of Nafion", *Phys. Chem. Chem. Phys.*, Vol. 10 (2008), pp. 5678-5688.

(32) Osher, S. and Fedkiw, R., *Level Set Methods and Dynamic Implicit Surfaces* (2003), Springer.

(33) Lallemand, P. and Luo, L. -S., "Theory of the Lattice Boltzmann Method: Dispersion, Dissipation, Isotropy, Galilean Invariance, and Stability", *Phys. Rev. E*, Vol. 61 (2000), pp. 6546-6562.

(34) d'Humières, D., Ginzburg, I., Krafczyk, M., Lallemand, P. and Luo, L. -S., "Multiple-relaxation-time Lattice Boltzmann Models in Three Dimensions", *Philos. Trans. R. Soc. Lond. A*, Vol. 360 (2002), pp. 437-451.

(35) Guo, Z., Zheng, C. and Shi, B. C., "Lattice Boltzmann Equation with Multiple Effective Relaxation Times for Gaseous Microscale Flow", *Phys. Rev. E*, Vol. 77 (2008), 036707.

(36) Dawson, S. P., Chen, S. and Doolen, G. D., "Lattice Boltzmann Computations for Reaction-diffusion Equations", *J. Chem. Phys.*, Vol. 98 (1993), pp. 1514-1523.

(37) Junk, M., Klar, A. and Luo, L. -S., "Asymptotic Analysis of the Lattice Boltzmann Equation", *J. Comput. Phys.*, Vol. 210 (2005), pp. 676-704.

(38) Junk, M. and Yang, Z., "Asymptotic Analysis of Lattice Boltzmann Boundary Conditions", *J. Stat. Phys.*, Vol. 121 (2005), pp. 3-35.

(39) Caiazzo, A., Junk, M. and Rheinländer, M., "Comparison of Analysis Techniques for the Lattice Boltzmann Method", *Comput. Math. Appl.*, Vol. 58 (2009), pp. 883-897.

(40) Sussman, M., Fatemi, E., Smereka, P. and Osher, S., "An Improved Level Set Method for Incompressible Two-phase Flows", *Comput. Fluids*, Vol. 27 (1998), pp. 663-680.

(41) Flin, F., Brzoska, J. B., Coeurjolly, D., Pieritz, R. A., Lesaffre, B., Coléou, C., Lamboley, P., Teytaud, O., Vignoles, G. L. and Delesse, J. F., "Adaptive Estimation of Normals and Surface Area for Discrete 3-D Objects: Application to Snow Binary Data from X-ray Tomography", *IEEE Trans. Image Process.*, Vol. 14 (2005), pp. 585-596.

(42) Yoshida, H. and Nagaoka, M., "Multiple-relaxation-time Lattice Boltzmann Model for the Convection and Diffusion Equation and Its Applications", *Abstracts of the 8th International Conference for Mesoscopic Methods in Engineering and Science* (2011), p. 18., National Institute of Applied Sciences.

(43) Yoshida, H., Baba, N., Nagaoka, M., Kawauchi, S. and Itou, Y., "Numerical Analysis of Ion Transport in Electrodes of Lithium Ion Secondary Batteries by Means of the Lattice Boltzmann Method", *Proceedings of the 51st Battery Symposium in Japan* (in Japanese), (2010), p. 80., The Electrochemical Society of Japan.

Figs. 2 - 7
Text
  p.69 left l.1 - right l.17
  p.70 left l.5 - l.24
  p.73 left l.10 - right l.10
  p.74 left l.5 - p.76 left l.27
  p.77 left l.3 - l.20

Hiroaki Yoshida
  Research Fields:
    - Computational Fluid Dynamics
    - Electrokinetic Flows
    - Modeling and Simulation of Electrochemical Processes
    - Multi-scale Simulation of Suspensions
  Academic Degree: Dr.Eng.
  Academic Societies:
    - The Japan Society of Mechanical Engineers
    - The Japan Society of Fluid Mechanics
  Award:
    - Certificate of Merit for Best Technological Presentation, The Japan Society of Mechanical Engineers, Computational Mechanics Division, 2011

Makoto Nagaoka
  Research Fields:
    - Computational Fluid Dynamics
    - Internal Combustion Engine
    - CAE
    - Modeling-Simulation-Optimization Process Development
  Academic Degree: Dr.Eng.
  Academic Societies:
    - Society of Automotive Engineers of Japan
    - The Japan Society of Mechanical Engineers
    - Institute for Liquid Atomization and Spray Systems-Japan
  Awards:
    - Paper Award, Japan Society of Automotive Engineers, 1992
    - SAE Arch T. Colwell Merit Award, 1996
    - Incentive Award, Japan Society of Mechanical Engineers, 1997